

# Enhance Control Performance of a Pneumatic Artificial Muscle System Using RBF-Neural Network Approximation and Power Rate Exponential Reaching Law Sliding Mode Control

Viet-Thanh Nguyen<sup>1</sup> and Quy Thinh Dao<sup>1,\*</sup>

<sup>1</sup>*School of Electrical and Electronic Engineering, Hanoi University of Science and Technology*

\**Corresponding author E-mail: [thinh.daoquy@hust.edu.vn](mailto:thinh.daoquy@hust.edu.vn)*

## Abstract

This research focuses on the integration of a radial basis function neural network (RBFNN) for uncertainty approximation in pneumatic artificial muscle (PAM) systems within the framework of power rate exponential reaching law sliding mode control (PRERL-SMC). Configured in an antagonistic manner, PAMs provide a range of benefits for developing actuators with human-like characteristics. Nevertheless, their intrinsic nonlinearity and uncertain behavior are obstacles to attaining accurate control, particularly in rehabilitation scenarios where ensuring control precision is imperative for safety and effectiveness. The proposed method leverages a power rate exponential reaching law to ensure chattering-free control and swift convergence towards desired trajectories, while the RBFNN effectively approximates system uncertainties. Through comprehensive experiments, we compare the RBF-PRERL-SMC approach with conventional control methods, showcasing its superior performance in tracking various trajectories. Notably, our strategy proves robust against external perturbations, demonstrating its applicability in rehabilitation scenarios.

**Keywords:** *Pneumatic artificial muscle, Discrete-time sliding mode control, Exponential reaching law, Radial basis function neural network.*

## 1. Introduction

The field of robotics has witnessed remarkable advancements in recent years, with applications ranging from industrial automation to healthcare. Among these innovations, pneumatic artificial muscle (PAM) systems have emerged as promising candidates for creating bio-inspired actuators capable of human-like motions. PAMs, known for their lightweight, cylinder shape, high power-to-weight ratio, low cost, ease of maintenance, cleanliness, and compliant nature, hold great promise in fields like prosthetics, exoskeletons, and rehabilitation [1, 2, 3, 4]. However, their nonlinear behavior and inherent uncertainty have posed significant challenges for achieving precise and adaptive control, particularly in scenarios where safety and effectiveness are paramount. Thanks to its robustness, adaptability, and ease of implementation, the sliding mode control theory has gained prominence across various domains of control and automation. This approach proves especially effective in managing intricate nonlinear models like the PAM system, renowned for its inherent nonlinearity. Nonetheless, conventional sliding-mode controllers might encounter challenges in delivering satisfactory performance when dealing with PAM systems exhibiting underactuated attributes. The concept of sliding mode control (SMC) comprises two fundamental modes, namely the reaching phase and the sliding phase [5, 6]. In the reaching mode, the system trajectory progres-

sively approaches the predefined switching surface within a finite-time. Following this, during the sliding mode, the trajectories exhibit a distinct “sliding” behavior, smoothly converging towards the origin within the phase plane. A key challenge in SMC is chattering, resulting from rapid and high-frequency control signal switching. Chattering poses significant risks in real-time systems, potentially causing actuator wear and damage, making it undesirable. The issue of chattering in sliding mode control has garnered substantial attention within the research landscape, evident from the variety of strategies proposed in references [7, 8, 9, 10, 11, 12, 13, 14]. Furthermore, the intricate nature and inherent uncertainties inherent in PAM systems present substantial hurdles when developing efficient controllers. Consequently, there exists a significant demand for adaptive and intelligent algorithms that can complement and enhance the sliding mode control strategy.

In recognition of this challenge, researchers have been actively exploring novel approaches to enhance control quality and overcome the limitations of conventional controllers within the context of PAM systems. For instance, the work presented in [15] introduced a control design based on reinforcement learning for a pneumatic gearbox actuator. Similarly, modern and adaptive methodologies have been applied to PAM systems, such as model-free techniques employed for gripper fingers [16], as well as adaptive controllers tailored for PAM subjects [17, 18, 19, 20]. Additionally, the integration of fuzzy logic

control, known for its adeptness in handling complex systems, has been extensively explored in conjunction with conventional methods to enhance control quality [21, 22, 23, 24, 25, 26, 27], among others.

However, when confronted with the unique challenges posed by highly nonlinear and uncertain PAM systems, the necessity for an intelligent algorithm endowed with distinct capabilities such as approximation, adaptivity, and generalization becomes evident. The radial basis function neural network (RBFNN) emerges as a promising solution, excelling in the realms of automation and control. Its ability to model and approximate intricate nonlinear systems while maintaining robustness renders it particularly suitable. Notably, a recent study by Gendi Liu *et al.* showcased the application of neural networks for tracking control of a dual-PAM arm robot, culminating in successful hardware experiments on a real PAM humanoid actuator model [28]. The amalgamation of the RBFNN and sliding mode control methods holds significant promise, capitalizing on the individual strengths of each. The RBF-SMC method, underpinned by theoretical advancements [29], has also been effectively employed in diverse control contexts, including servo motors [30] and robotic systems [31, 32, 33].

In this study, the proposed improvement strategy is using RBF neural networks to approximate the uncertain parameters inherent in an antagonistic configuration of PAMs based on the framework of a sliding mode control method enhanced by PRERL. Integrating RBFNN and PRERL-SMC is crucial for effectively addressing challenges in controlling PAM systems, especially those with underactuated characteristics. The intrinsic nonlinearity of PAM systems can complicate control tasks that conventional sliding-mode controllers struggle to handle. RBFNNs excel in approximating PAM system uncertainties, enhancing adaptability and control precision. Meanwhile, PRERL-SMC offers chattering-free control and rapid convergence to desired trajectories, vital for accurate and smooth control actions.

In summary, this research offers valuable contributions that significantly enhance control performance within the realm of PAM systems. Primarily, it introduces an adaptive control mechanism, purposefully crafted to proficiently manage the often challenging antagonistic configurations present in PAMs. This is achieved through the integration of RBFNN and the innovative PRERL-SMC. Moreover, the paper provides compelling evidence of the practicality and high potential impact of this hybrid approach by showcasing extensive experimental results conducted under diverse conditions. These results, collectively demonstrating the effectiveness and suitability of the proposed method, strongly emphasize its relevance and applicability in the domain of rehabilitation applications.

The paper is structured as follows: Section 2 outlines the experimental setup and the mathematical model of the PAM system. In Section 3, the design and stability analysis of the proposed RBF-PRERL-SMC controller are discussed. Section 4 presents the experimental results validating the effectiveness of the proposed approach. Finally, Section 5 concludes the paper by summarizing contributions and suggesting potential future research directions.

## 2. System modeling

The PAM-based experiment setup is shown in Figure 1, with its diagram presented in Figure 2. This configuration consists of a pair of self-made pneumatic artificial muscle actuators, arranged antagonistically, with a diameter of  $23 \times 10^{-3}$  (m) and a nominal length of  $40 \times 10^{-2}$  (m). The internal pressure of the pneumatic artificial muscle actuators is regulated via a proportional valve from SMC company, resulting in the rotational motion of a pulley wheel. A WDD35D8T angular sensor quantifies this rotational motion. The control system for this configuration utilizes the National Instruments myRIO-1900 embedded controller to process angle potentiometer data and deliver control signals to proportional valves. LabVIEW software is employed to interface, supervise, and monitor the complete experimental procedure.

Given the antagonistic system configuration illustrated in Figure 2, in which the internal pressures of the two PAMs can be described as follows:

$$\begin{cases} P_1 = P_0 + \Delta P \\ P_2 = P_0 - \Delta P \end{cases} \quad (1)$$

where  $P_0$  denotes the PAMs' initial pressure, and  $\Delta P$  represents the changed pressure.

The control voltages for regulating the PAMs' proportional valves are formulated as follows:

$$\begin{cases} u_1 = u_0 + u = k_0(P_0 + \Delta P) \\ u_2 = u_0 - u = k_0(P_0 - \Delta P) \end{cases} \quad (2)$$

$u_0$  signifies the preloaded voltage, while  $k_0$  relates the output pressure of pneumatic artificial muscles (PAMs) to the control voltage  $u$ . The variable  $u$  becomes the manipulated parameter, acting as the control input for the closed-loop system, governing PAM contraction and consequently altering the joint angle  $\theta$ . The deflection angle signal is then conveyed back through a sensor, establishing a correlation where antagonistic PAM pairs function as a single-input single-output system. Here, the control voltage  $u$  from the Myrio controller serves as the input, while the measured pulley's angle  $\theta$  becomes the output. For this type of control system, a linear model characterizes the system's behavior, with any residual modeling error considered a lumped disturbance and managed by the controller. In our investigation, leveraging input/output data and a series of experiments, we adopt a discrete-time second-order mathematical model with perturbation as the representation of the

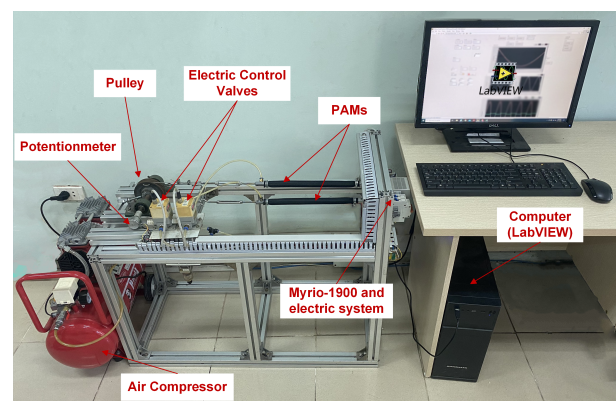


**Figure 1.** Experiment Platform of PAM-Based Antagonistic Configuration.



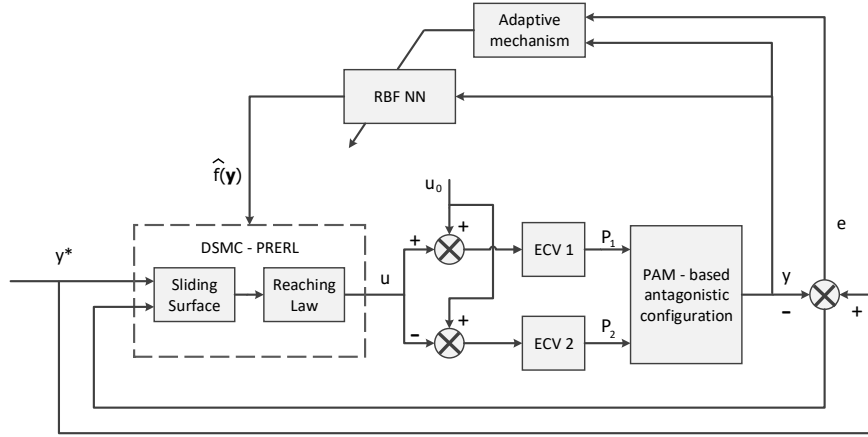


Figure 3. Block diagram of the system controller.

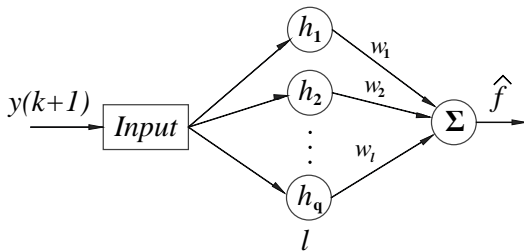


Figure 4. The 1-q-1 RBFNN structure.

**Remark 1.** If  $\delta_0$  is set to one and  $\alpha$  is set to zero, the resultant controller transforms into the DSMC with a constant rate reaching law. This implies that the conventional reaching law is a specific instance of the introduced method.

Afterward, the proposed control signal is obtained by inserting the sliding variable  $s_{k+1}$  from equation (10) into equation (9), and subsequently solving for  $u_k$ . This yields:

$$u_k = \frac{1}{b_1} \left\{ y^*(k+1) + f(y(k)) - \sum_{j=2}^m b_j u(k-j+1) + \lambda [y^*(k) - y(k)] - s(k) + \frac{\gamma}{\Psi(k)} |s(k)|^\alpha \operatorname{sgn}(s(k)) \right\} \quad (12)$$

### 3.3. RBF neural network design

At Eq. 12, since the element  $f(y)$  is unknown and uncertain due to the system's characteristics, we utilized radial-basis-function neural network to approximate  $f(y)$ . To increase control accuracy and adjust to parameter fluctuations, this work aims to introduce an SMC strategy combined with the RBFNN for uncertainty estimation purposes and simultaneously apply it to the PAM configuration.

In this study, the 1-q-1 radial basis function neural network (RBFNN) architecture (Figure 4) is employed to approximate the function  $f(\cdot)$  using the subsequent algorithm:

$$\hat{f}(y(k)) = \hat{\mathbf{w}}(k)^T \mathbf{h}(y(k-1)) \quad (13)$$

where the selection of the value  $y(k-1)$  serves as the input to the network,  $\hat{\mathbf{w}}(k)$  represents the vector containing the network's weight values. The vector  $\mathbf{h} = [h_l]^T$  corresponds to the output of the Gaussian function, with each component  $h_l$  being defined in a subsequent manner

$$h_l = \exp\left(-\frac{\|y(k-1) - p_l\|^2}{b_l^2}\right) \quad (14)$$

where

$$p = [p_l] = [p_1, p_2, \dots, p_q]$$

represents the positional value of the Gaussian function's center point within the neural network. This vector consists of a single row that corresponds to the number of elements in the input. The index  $l$ , ranging from 1 to  $q$ , signifies the hidden layer node number. Additionally, the Gaussian function's spread for node  $l$  is denoted by the vector  $b = [b_l] = [b_1, \dots, b_q]^T$ . For any non-zero value of the approximation error bound  $\varepsilon_f$ , there exist specific optimal weight vectors  $\mathbf{w}^*$  such that:

$$f(y) = \hat{f}(y, \mathbf{w}^*) - \Delta_f(y) \quad (15)$$

where  $\Delta_f(y)$  represents the optimal network approximation error, and  $|\Delta_f(y)| < \varepsilon_f$ . Subsequently, we can derive the general network approximation error as follows:

$$\begin{aligned} \tilde{f}(y(k)) &= f(y(k)) - \hat{f}(y(k)) \\ &= \hat{f}(y(k), \mathbf{w}^*) - \Delta_f(y(k-1)) - \hat{\mathbf{w}}(k)^T \mathbf{h}(y(k-1)) \\ &= -\tilde{\mathbf{w}}(k)^T \mathbf{h}(y(k-1)) - \Delta_f(y(k-1)) \end{aligned} \quad (16)$$

where  $\tilde{\mathbf{w}}(k) = \hat{\mathbf{w}}(k) - \mathbf{w}^*$ . With the estimated component  $\hat{f}(y(k))$ , the control law at (12) is rewritten as:

$$u(k) = \frac{1}{b_1} \left\{ y^*(k+1) + \hat{f}(y(k)) - \sum_{j=2}^m b_j u(k-j+1) + \lambda [y^*(k) - y(k)] - s(k) + \frac{\gamma}{\Psi(k)} |s(k)|^\alpha \operatorname{sgn}(s(k)) \right\} \quad (17)$$

Assuming that the sliding surface (10) is approached, it means  $s(k) \rightarrow 0$ , substituting (17) into (4), we have:

$$\begin{aligned} y^*(k+1) - y(k+1) &= f(y(k)) - \hat{f}(y(k)) - \lambda [y^*(k) - y(k)] \\ e(k+1) &= \tilde{f}(y(k)) - \lambda e(k) \end{aligned}$$

Thus,

$$e(k) + \lambda e(k-1) = \tilde{f}(\mathbf{y}(k-1)) \quad (18)$$

The expression for (18) can also be represented as:

$$e(k) = \Gamma^{-1}(z^{-1})\tilde{f}(\mathbf{y}(k-1)) \quad (19)$$

where  $\Gamma^{-1}(z^{-1}) = 1 + \lambda z^{-1}$ ,  $z^{-1}$  is the discrete-time delay operator. Introduce a novel augmented error denoted as:

$$e_1(k) = \eta[e(k) - \Gamma^{-1}(z^{-1})v(k)] \quad (20)$$

where  $\eta > 0$ .

By replacing (19) into (20), we obtain:

$$\begin{aligned} e_1(k) &= \eta\Gamma^{-1}(z^{-1})[\tilde{f}(\mathbf{y}(k-1)) - v(k)] \\ &= \eta \frac{1}{1 + \lambda z^{-1}} [\tilde{f}(\mathbf{y}(k-1)) - v(k)] \end{aligned}$$

resulting in the relationship:

$$e_1(k-1) = \frac{\eta[\tilde{f}(\mathbf{y}(k-1)) - v(k)] - e_1(k)}{\lambda} \quad (21)$$

The auxiliary signal  $v(k)$  is designed in such a way that the convergence of  $e_1(k) \rightarrow 0$  implies the convergence of  $e(k) \rightarrow 0$ . The design of the auxiliary signal is based on a well-established theory described in [36]:

$$v(k) = v_1(k) + v_2(k)$$

with  $v_1(k) = \frac{\eta}{2\mu\lambda^2} \mathbf{h}^T(\mathbf{y}(k-1))e_1(k)$  and  $v_2(k) = Ge_1(k)$ . ( $G$  is a positive constant)

From (20), we obtain

$$e_1(k) = \eta \left[ e(k) - \frac{1}{1 + \lambda z^{-1}} v(k) \right] \quad (22)$$

or

$$e_1(k) \times (1 + \lambda z^{-1}) = \eta [e(k)(1 + \lambda z^{-1}) - v(k)] \quad (23)$$

Therefore,

$$e_1(k) = -\lambda e_1(k-1) + \eta [e(k) + \lambda e(k-1) - v(k)] \quad (24)$$

Let's consider  $v(k)$  as a virtual variable, define  $v'_1(k) = \frac{\eta}{2\mu\lambda^2} \mathbf{h}^T(\mathbf{y}(k-1))\mathbf{h}(\mathbf{y}(k-1))$ , then we have  $v(k) = [v'_1(k) + G]e_1(k)$ . Blending in (24), we received:

$$e_1(k) = \frac{-\lambda e_1(k-1) + \eta [e(k) + \lambda e(k-1)]}{1 + \eta [v'_1(k) + G]} \quad (25)$$

The adaptive law is designed as:

$$\Delta \hat{\boldsymbol{\omega}}(k) = \begin{cases} \frac{\eta}{\mu\lambda^2} \mathbf{h}(\mathbf{y}(k-1))e_1(k) & \text{if } |e_1(k)| > \varepsilon_f/G \\ 0 & \text{if } |e_1(k)| \leq \varepsilon_f/G \end{cases} \quad (26)$$

where  $\Delta \hat{\boldsymbol{\omega}}(k) = \hat{\boldsymbol{\omega}}(k) - \hat{\boldsymbol{\omega}}(k-1)$ ,  $\mu$  and  $G$  are constants strictly greater than zero.

### 3.4. Stability analysis

In this section, we will theoretically prove the behavior of the sliding function as depicted in the proposed reaching law (10).

**Lemma 1.** Defining a positive function  $\Phi(\alpha)$  as

$$\Phi(\alpha) = 1 + \alpha^{\frac{1}{1-\alpha}} - \alpha^{\frac{1}{1-\alpha}} \quad (27)$$

in which  $1 < \Phi(\alpha) < 2$  if  $0 < \alpha < 1$  [37].

**Theorem 1.** For the discrete-time SISO system (3) along with the sliding surface (5) and the controller (12), the assurance is provided that the sliding variable  $s(k)$  will enter the finite-time region  $\Omega$ , which is defined as:

$$\Omega = \left\{ |s(k)| \leq \Phi(\alpha) \frac{\gamma}{\Psi(k)}^{\frac{1}{1-\alpha}} \right\} \quad (28)$$

*Proof.* Designing Lyapunov function  $V(k) = [s(k)]^2$  and base on (10), one obtains

$$\begin{aligned} \Delta V(k) &= V(k+1) - V(k) \\ &= - \left[ \frac{\gamma}{\Psi(k)} |s(k)|^\alpha \operatorname{sgn}(s(k)) \right] \times \\ &\quad \left[ 2s(k) - \frac{\gamma}{\Psi(k)} |s(k)|^\alpha \operatorname{sgn}(s(k)) \right] \end{aligned} \quad (29)$$

If  $s(k) \notin \Omega$ , there will have two cases for  $s(k)$ .

**Case 1.**  $s(k) > \Phi(\alpha) \frac{\gamma}{\Psi(k)}^{\frac{1}{1-\alpha}} > 0$

In this case, it can be derived that

$$[s(k)]^{1-\alpha} > [\Phi(\alpha)]^{1-\alpha} \frac{\gamma}{\Psi(k)} \quad (30)$$

which results in

$$[s(k)]^\alpha [s(k)]^{1-\alpha} > [s(k)]^\alpha [\Phi(\alpha)]^{1-\alpha} \frac{\gamma}{\Psi(k)} \quad (31)$$

Since  $[\Phi(\alpha)]^{1-\alpha} > 1$ , the following deduction can be held

$$s(k) > |s(k)|^\alpha \frac{\gamma}{\Psi(k)} \operatorname{sgn}(s(k)) > 0 \quad (32)$$

which implies

$$2s(k) - \frac{\gamma}{\Psi(k)} |s(k)|^\alpha \operatorname{sgn}(s(k)) > 0 \quad (33)$$

Thus, in both observation of (29), (32), and (33), it becomes

$$\Delta V(k) = V(k+1) - V(k) < 0 \quad (34)$$

**Case 2.**  $s(k) < -\Phi(\alpha) \frac{\gamma}{\Psi(k)}^{\frac{1}{1-\alpha}} < 0$

By conducting a similar analysis, it can be deduced that  $\Delta V(k) < 0$  remains valid. As a result, the sliding variable  $s(k)$  will indeed enter the domain  $\Omega$  within a finite number of steps. This concludes the proof.  $\square$

**Lemma 2.** Mentioned function  $\Phi(\alpha)$  in (27), if  $0 < \alpha < 1$ , then  $\theta\Phi(\alpha) - \theta^\alpha[\Phi(\alpha)]^\alpha + \Phi(\alpha) - 1 \geq 0$  for any  $\theta \in [0, 1]$ .

*Proof.* Define  $g(\theta) = \theta\Phi(\alpha) - \theta^\alpha[\Phi(\alpha)]^\alpha + \Phi(\alpha) - 1$ .

First, since Lemma 1 implies  $1 < \Phi(\alpha) < 2$  if  $0 < \alpha < 1$ , we can easily infer that  $g(0) = \Phi(\alpha) - 1 > 0$  and  $\Phi(\alpha) - [\Phi(\alpha)]^\alpha > 0$ , which also remains  $g(1) = \Phi(\alpha) - [\Phi(\alpha)]^\alpha + \Phi(\alpha) - 1 > 0$ .

Secondly, by solving  $g(\theta) = 0$  to determine the critical points of  $g(\theta)$ , we obtain:

$$\Phi(\alpha) - \alpha\theta^{\alpha-1}\Phi(\alpha)^\alpha = 0 \quad (35)$$

which follows  $\theta^{1-\alpha} = \alpha\Phi(\alpha)^{-(1-\alpha)}$  then  $\theta = [\alpha^{1-\alpha}/\Phi(\alpha)]$ .

By substituting it into  $g(\theta)$ , we arrive at  $g(\theta) = 0$  with the critical point  $\theta = \alpha^{1-\alpha}/\Phi(\alpha)$ . Considering the values of  $g(0)$  and  $g(1)$  as well, it can be concluded that  $\min_{\theta \in [0,1]} g(\theta) = 0$ . This concludes the proof of Lemma 2.  $\square$

**Theorem 2.** *Once  $s(k)$  enters the region  $\Omega$ , it remains confined within it and cannot exit.*

*Proof.* Suppose  $s(k) = \theta\Phi(\alpha) \left(\frac{\gamma}{\Psi(k)}\right)^{\frac{1}{1-\alpha}}$  with  $0 \leq \theta \leq 1$ . By considering the reaching law (10), we can deduce that

$$\begin{aligned} s(k+1) &= \theta\Phi(\alpha) \frac{\gamma}{\Psi(k)} \frac{1}{1-\alpha} - (\theta\Phi(\alpha))^\alpha \frac{\gamma}{\Psi(k)} \frac{1}{1-\alpha} \\ &= \left[1 - (\theta\Phi(\alpha))^{\alpha-1}\right] \theta\Phi(\alpha) \frac{\gamma}{\Psi(k)} \frac{1}{1-\alpha} \end{aligned} \quad (36)$$

Since  $\theta\Phi(\alpha) \geq 0$ ,  $\left[1 - (\theta\Phi(\alpha))^{\alpha-1}\right] \leq 1$ . Thus, we can derive from (36) the following expression:

$$s(k+1) \leq \Phi(\alpha) \frac{\gamma}{\Psi(k)} \frac{1}{1-\alpha} \quad (37)$$

Beside, examining (36) provides:

$$s(k+1) = \left[\theta\Phi(\alpha) - (\theta\Phi(\alpha))^\alpha\right] \frac{\gamma}{\Psi(k)} \frac{1}{1-\alpha} \quad (38)$$

Considering the range of  $0 < \alpha < 1$ , if  $\theta\Phi(\alpha) \geq 1$ , then  $\theta\Phi(\alpha) - (\theta\Phi(\alpha))^\alpha > 0$ . Moreover, if  $0 \leq \theta\Phi(\alpha) \leq 1$ , it can be deduced from Lemma 2 that:  $\theta\Phi(\alpha) - \theta^\alpha\Phi(\alpha)^\alpha \geq 1 - \Phi(\alpha) \geq -\Phi(\alpha)$ . Hence, based on the range of  $0 \leq \theta \leq 1$ , it can be concluded that:

$$s(k+1) \geq -\Phi(\alpha) \frac{\gamma}{\Psi(k)} \frac{1}{1-\alpha} \quad (39)$$

Consequently, it can be deduced from (37) and (39) that when  $s(k) \in \Omega$ , the state  $s(k+1) \in \Omega$ . A similar outcome can be derived under the assumption:  $s(k) = \theta\Phi(\alpha) \frac{\gamma}{\Psi(k)} \frac{1}{1-\alpha}$  with  $-1 \leq \theta \leq 0$ , which results in  $s(k+1) \in \Omega$ . As a consequence, the sliding variable will remain within the region  $\Omega$  subsequent to its entry.

This completes the proof.  $\square$

**Remark 2.** *In the context of the power rate method, the presence of the condition  $0 < \alpha < 1$  is crucial. However, it's worth noting that when  $\alpha$  takes a relatively high value, the sliding mode motion might not occur. While this can lead to rapid reaching of the equilibrium point, it also tends to negatively impact the system's robustness. As a result, it's recommended to choose  $\alpha$  within the range of  $0 < \alpha < 0.5$ , a suggestion put forth in [35].*

## 4. Experimental results

This section delves into the assessment of the effectiveness of the introduced controller in achieving the desired trajectories. The experimentation was conducted using the NI-Myrio 1900 microcontroller along with the NI LabVIEW software application. To implement the control algorithm, a discrete sampling time of 5 milliseconds ( $T_s$ ) was chosen. Furthermore, the main purpose of this study is to provide accreditation for the enhancement of radial-basis-function neural networks (RBFNN). The comparison involves evaluating the suggested control method against an exponential reaching law discrete-time sliding mode controller (PRERL - DSMC) without the use of the RBFNN technique. This evaluation is conducted based on performance criteria under identical operating conditions. The model parameters for the PAMs system are provided in Table 1. Besides, the control parameters for the PRERL technique are fine-tuned through trial and are detailed in Table 2. Notably, PRERL-SMC base common parameters between the two controllers being compared are kept consistent.

**Table 2.** Parameters of the PRERL technique

Parameters	$\lambda$	$\gamma$	$\delta_0$	$\beta$	$p$	$\alpha$
Values	0.5	3	0.2	0.05	1	0.4

Due to the intricate nature of the system, we opted for a 1-7-1 configuration for the RBF neural network. In this setup, the input of the neural network consists of a single node representing the measured joint angle. The hidden layer is composed of 7 nodes to encompass the span of the signal and compute weight vectors effectively. The width value  $\mathbf{b}$  is determined to offer optimal efficacy. The output layer includes a single node that signifies the approximated parameter  $f(x)$  of the PAM object. The parameters of the RBFNN adaptive method display as follows:

$$\begin{aligned} \mathbf{p} &= [-40 \quad -20 \quad -10 \quad 0 \quad 10 \quad 20 \quad 40], \\ \mathbf{b} &= [2, 2, 2, 2, 2, 2, 2], \\ \eta &= 0.05, G = 5000, \varepsilon_f = 0.03, \mu = 0.03. \end{aligned}$$

Following that, experiments were undertaken to assess the performance of the suggested controller in two distinct tasks: tracking the intersection of sinusoidal trajectories and tracking gait trajectories.

### 4.1. Tracking the conjuncture of sinusoidal signals

In this part, the required trajectories are made up of several signals. Consequently, a combination of three sinusoidal signals, each possessing distinct amplitudes and frequencies, is employed to form the reference signal. The equation describing the reference trajectory is determined as follows:

$$y^*(k) = A \sin(2\pi f \times kT_s) + 0.5A \sin(2\pi 0.1 \times kT_s) + 0.2A \sin(2\pi 0.5 \times kT_s), \text{ with } T_s = 0.005(s)$$

During the practical experimentation, the base amplitude is set at  $A = 30^\circ$ , and the base frequency  $f$  is tested at both  $0.2Hz$  and  $0.3Hz$ . The experiment outcomes with  $f = 0.3Hz$  are depicted in Figure 5. The upper and lower sub-figures correspondingly display the tracking performance and tracking error.

The results from these scenarios illustrate the outstanding tracking capabilities of the proposed controller. The MTE is around  $3.0^\circ$ , ensuring a satisfactory level of accuracy. Compared to the

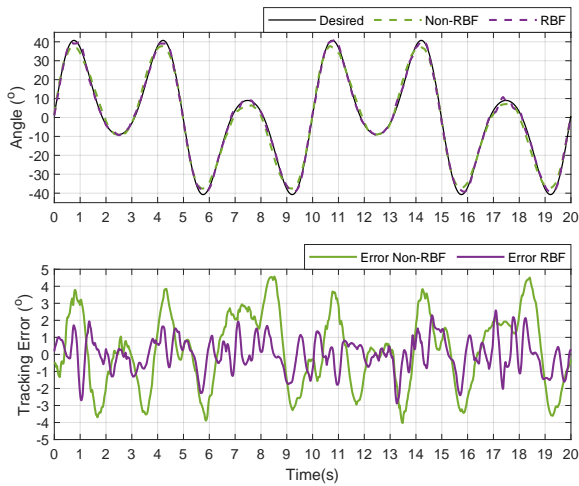


**Figure 5.** Experiment results when tracking combined sinusoidal trajectory with 0.3Hz of basis frequency.

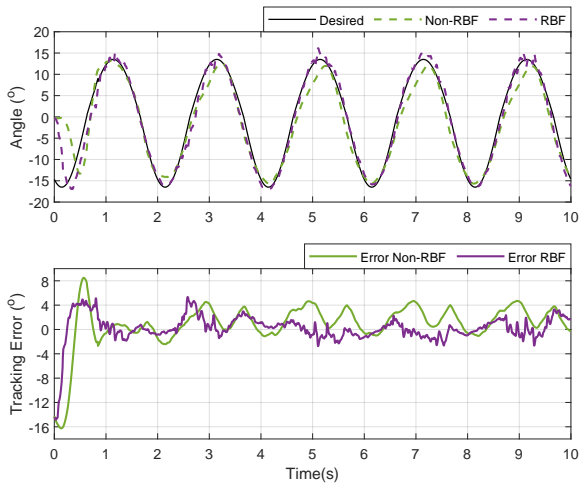


**Figure 6.** Experiment results when tracking 0.5Hz hip trajectories.

PRERL-SMC, the RBF-PRERL-SMC demonstrates significant superiority, particularly when dealing with high-angle rates of change. The RBF-PRERL-SMC maintains robust and accurate tracking performance, while the simpler controller exhibits lower accuracy, with a maximum tracking error of approximately  $6.0^\circ$ , which is twice as high as that of the proposed controller. Examining the root-mean-square error (RMSE) statistics, presented in Table 3, it is evident that the RBF-PRERL-SMC controller achieves an RMSE of approximately  $1.1^\circ$ , which is twice as good as its counterpart with an RMSE value of about  $2.5^\circ$ .

#### 4.2. Tracking gait-pattern signals

To evaluate the system's tracking capacity for rehabilitation applications, we examined its performance using gait trajectories. We utilized human gait data obtained from a prior study [38] to generate reference signals for the hip and knee joints, which were subsequently employed in our experiments. The outcomes of the experiments, focused on tracking the hip and knee trajectories, are depicted in Figures 6 and 7, respectively. In the case of the hip joint, the intended angle range encompasses values between  $-16.5^\circ$  and  $+13.5^\circ$ , while for the knee

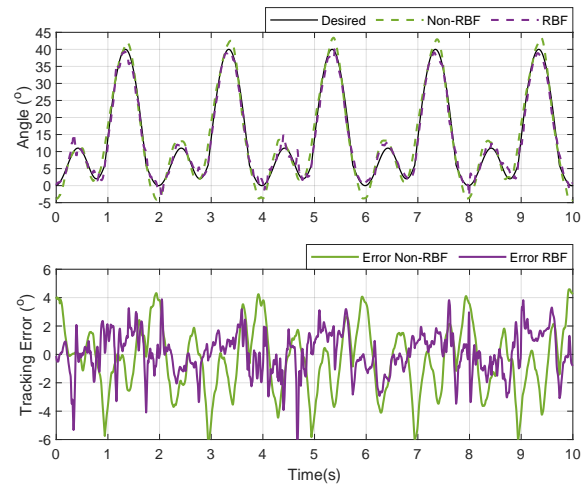


**Figure 7.** Experiment results when tracking 0.5Hz knee trajectories.

**Table 3.** RMSE of two controllers at combined sinusoidal signals experiment.

Basis frequency	Non-RBF	RBF
0.2	2.25	1.10
0.3	2.40	1.00

joint, it varies between  $0.0^\circ$  and  $+40.0^\circ$ . All the specified desired trajectories were executed at frequencies of  $0.2\text{Hz}$  and  $0.5\text{Hz}$ .

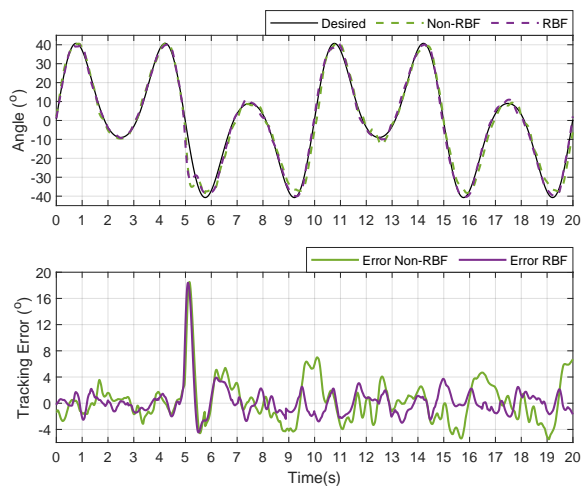
The experiment has been successfully conducted, and stability has been achieved in all tested scenarios. When evaluated based on the Maximum Tracking Error (MTE) criteria, there is no significant difference between the RBF-PRERL-SMC and the conventional controller when tracking hip joint trajectories, as the MTEs of both controllers are approximately  $16^\circ$ . This is due to the non-zero initial angle of the desired signal, while the actual angle is initially set as zero (as shown in Figure 6). However, the RBF-PRERL-SMC controller exhibits a faster convergence speed and lower error. The superior performance of the RBF-PRERL-SMC method is also evident from the RMSE criteria presented in Table 4. While tracking the hip joint trajectory, the performance of the conventional method deteriorates rapidly (RMSE values is  $3.27^\circ$  at  $0.5\text{Hz}$ ). In contrast, the with-RBF method maintains a high level of tracking ability with RMSEs of  $2.28^\circ$  at  $0.5\text{Hz}$ . Similar results are observed for the knee joint.

#### 4.3. Tracking experiments with external disturbances

For rehabilitation, it is crucial to thoroughly examine the robustness and stability of the system thoroughly. In practical scenarios, the presence of disturbances cannot be overlooked, as they inevitably affect control performance. To simulate such conditions, we conducted experiments with the antagonistic PAM system horizontally set up. After the system had been operating smoothly for approximately 5 seconds, we introduced a sudden vertical load of ten kilograms. The experimental results under various conditions are illustrated in Figures 8 and 9. It becomes evident that an extremely heavy load disrupts stability almost immediately. The RBF-PRERL-SMC strategy takes

**Table 4.** RMSE (°) of two controllers when tracking gait-pattern signals

Gait's frequency	Hip joint		Knee joint	
	Non-RBF	RBF	Non-RBF	RBF
0.2 Hz	2.47	1.84	1.85	1.10
0.5 Hz	3.27	2.28	2.66	1.48

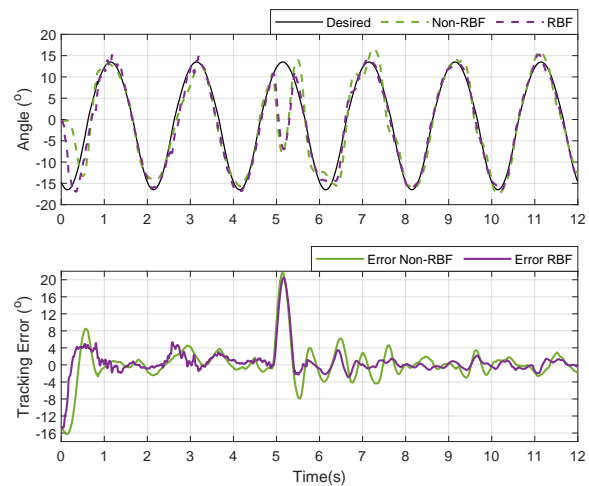
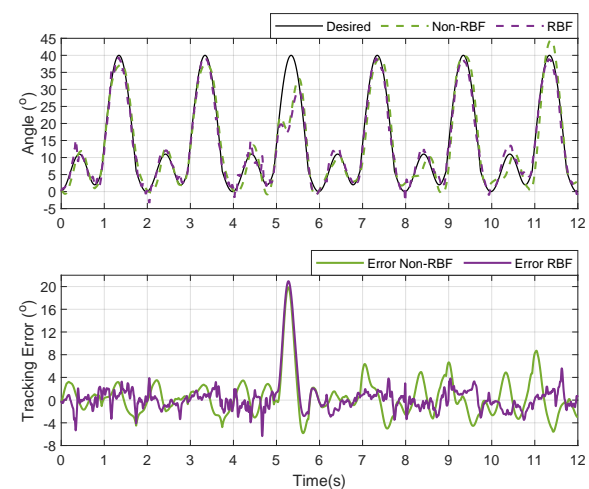
**Figure 8.** Experiment results when tracking combined sinusoidal trajectories with an external disturbance.

around 2 seconds to regain stability, while the non-RBF approach requires a significantly longer period or might even lose control quality. These results confirm that the system upgraded by the RBF technique can maintain equilibrium and endure substantial external disturbances. However, when subjected to a substantial disturbance, the control quality might experience a slight decline.

## 5. Conclusion and Discussion

In this study, we presented an enhanced discrete-time sliding mode control approach for pneumatic artificial muscle (PAM) systems. The integration of a radial basis function neural network (RBFNN) for uncertainty approximation, along with the utilization of power rate exponential reaching law sliding mode control (PRERL-SMC), has been shown to significantly improve the performance of PAM systems. The combination of these techniques addresses the inherent challenges posed by PAMs' nonlinearity and uncertainty, particularly in scenarios such as rehabilitation applications where precise control is essential for safety and effectiveness. The power rate exponential reaching law effectively suppressed chattering, ensuring smooth control actions and minimizing unnecessary oscillations. Furthermore, the RBFNN contributed to accurate uncertainty approximation, enhancing the overall control precision and adaptability of the system. The results obtained underscore the applicability of the proposed approach in real-world scenarios, showcasing its effectiveness in achieving robust and precise control. Notably, the proposed strategy exhibited robustness against external perturbations, which is crucial for maintaining control quality in real-world scenarios.

For forthcoming research, we intend to explore more advanced

**(a) Hip joint's trajectory.****(b) Knee joint's trajectory.****Figure 9.** Experiment results when tracking gait trajectories at 0.2Hz with an external disturbance.

RBF algorithms and integrate them with other control strategies to fully harness the potential of neural networks. This amalgamation aims to further elevate the system's performance and efficacy. Additionally, we plan to conduct targeted practical experiments tailored specifically to rehabilitation contexts.

## Acknowledgement

This research is funded by Hanoi University of Science and Technology (HUST) under project number T2022 - PC - 002

## References

- [1] Bhaben Kalita and S. K. Dwivedy. Dynamic analysis of pneumatic artificial muscle (pam) actuator for rehabilitation with principal parametric resonance condition - nonlinear dynamics. *SpringerLink*, Jul 2019.
- [2] Sai K. Banala, Seok Hun Kim, Sunil K. Agrawal, and John P. Scholz. Robot assisted gait training with active leg exoskeleton (alex). In *2008 2nd IEEE RAS & EMBS International Conference on Biomedical Robotics and Biomechatronics*, pages 653–658, 2008.
- [3] Quy-Thinh Dao and Shin-ichiroh Yamamoto. Assist-as-needed control of a robotic orthosis actuated by pneumatic artificial muscle for gait rehabilitation. *Applied Sciences*, 8(4), 2018.
- [4] Shahid Hussain, Sheng Q. Xie, and Prashant K. Jamwal. Control of a robotic orthosis for gait rehabilitation. *Robotics and Autonomous Systems*, 61(9):911–919, 2013.
- [5] Vadim I. Utkin. Sliding modes in control and optimization. In *Communications and Control Engineering Series*, 1992.

- [6] Roohma Afifa, Sadia Ali, Mahmood Pervaiz, and Jamshed Iqbal. Adaptive backstepping integral sliding mode control of a mimo separately excited dc motor. *Robotics*, 12(4), 2023.
- [7] Omer Saleem and Jamshed Iqbal. Fuzzy-immune-regulated adaptive degree-of-stability lqr for a self-balancing robotic mechanism: Design and hil realization. *IEEE Robotics and Automation Letters*, 8(8):4577–4584, 2023.
- [8] Sohail Ahmad, Ali Arshad Uppal, Muhammad Rizwan Azam, and Jamshed Iqbal. Chattering free sliding mode control and state dependent kalman filter design for underground gasification energy conversion process. *Electronics*, 12(4), 2023.
- [9] J.H. Lilly and P.M. Quesada. A two-input sliding-mode controller for a planar arm actuated by four pneumatic muscle groups. *IEEE Transactions on Neural Systems and Rehabilitation Engineering*, 12(3):349–359, 2004.
- [10] Cong Phat Vo, Xuan Dinh To, and Kyoung Kwan Ahn. A novel adaptive gain integral terminal sliding mode control scheme of a pneumatic artificial muscle system with time-delay estimation. *IEEE Access*, 7:141133–141143, 2019.
- [11] Chia-Jui Chiang and Ying-Chen Chen. Neural network fuzzy sliding mode control of pneumatic muscle actuators. *Engineering Applications of Artificial Intelligence*, 65:68–86, 2017.
- [12] Jean-Jacques E Slotine, Weiping Li, et al. *Applied nonlinear control*, volume 199. Prentice hall Englewood Cliffs, NJ, 1991.
- [13] Pushkin Kachroo and Masayoshi Tomizuka. Chattering reduction and error convergence in the sliding-mode control of a class of nonlinear systems. *IEEE Transactions on automatic control*, 41(7):1063–1068, 1996.
- [14] Leonid M Fridman. An averaging approach to chattering. *IEEE Transactions on Automatic Control*, 46(8):1260–1265, 2001.
- [15] Tamás Bécsi, Szilárd Aradi, Ádám Szabó, and Péter Gáspár. Policy gradient based reinforcement learning control design of an electro-pneumatic gearbox actuator. *IFAC-PapersOnLine*, 51(22):405–411, 2018.
- [16] Pol Hamon, Loïc Michel, Franck Plestan, and Damien Chablat. Control of a gripper finger actuated by a pneumatic muscle: new schemes based on a model-free approach. *IFAC-PapersOnLine*, 55(27):25–30, 2022.
- [17] Ling Zhao, Haiyan Cheng, Jinhui Zhang, and Yuanqing Xia. Adaptive control for a motion mechanism with pneumatic artificial muscles subject to dead-zones. *Mechanical Systems and Signal Processing*, 148:107155, 2021.
- [18] Jian Huang, Yu Cao, and Yan-Wu Wang. Adaptive proxy-based sliding mode control for a class of second-order nonlinear systems and its application to pneumatic muscle actuators. *ISA Transactions*, 124:395–402, 2022.
- [19] Minh-Duc Duong, Quang-Thuyet Pham, Tuan-Chien Vu, Ngoc-Tam Bui, and Quy-Thinh Dao. Adaptive fuzzy sliding mode control of an actuator powered by two opposing pneumatic artificial muscles. *Scientific Reports*, 13(1):8242, 2023.
- [20] Quy-Thinh Dao, Vuong Van Dinh, Chien Tuan Vu, Thuyet Quang Pham, and Duc Minh Duong. An adaptive sliding mode controller for a pam-based actuator. *Engineering, Technology & Applied Science Research*, 13(1):10086–10092, 2023.
- [21] S.W. Chan, J.H. Lilly, D.W. Repperger, and J.E. Berlin. Fuzzy pd+i learning control for a pneumatic muscle. In *The 12th IEEE International Conference on Fuzzy Systems, 2003. FUZZ '03.*, volume 1, pages 278–283 vol.1, 2003.
- [22] Ho Pham Huy Anh and Kyoung Kwan Ahn. Hybrid control of a pneumatic artificial muscle (pam) robot arm using an inverse narx fuzzy model. *Engineering Applications of Artificial Intelligence*, 24(4):697–716, 2011.
- [23] A. REZOUQ, F. HAMERLAIN, and M. HAMERLAIN. Application of fuzzy sliding mode to control of manipulator robot actuated by pneumatic artificial muscles. *IFAC Proceedings Volumes*, 42(19):580–585, 2009.
- [24] Cao Van Kien, Tran Thien Huan, Do Thanh Thai, and Ho Pham Huy Anh. Implementation of adaptive fuzzy sliding mode control for non-linear uncertain serial pneumatic-artificial-muscle (pam) robot system. In *2017 International Conference on System Science and Engineering (ICSSSE)*, pages 83–88, 2017.
- [25] Dingkun Liang, Ning Sun, Yiming Wu, Gendi Liu, and Yongchun Fang. Fuzzy-sliding mode control for humanoid arm robots actuated by pneumatic artificial muscles with unidirectional inputs, saturations, and dead zones. *IEEE Transactions on Industrial Informatics*, 18(5):3011–3021, 2022.
- [26] A. REZOUQ, F. HAMERLAIN, and M. HAMERLAIN. Application of fuzzy sliding mode to control of manipulator robot actuated by pneumatic artificial muscles. *IFAC Proceedings Volumes*, 42(19):580–585, 2009.
- [27] Huayang Sai, Zhenbang Xu, Ce Xu, Xiaoming Wang, Kai Wang, and Lin Zhu. Adaptive local approximation neural network control based on extraordinariness particle swarm optimization for robotic manipulators. *Journal of Mechanical Science and Technology*, 36(3):1469–1483, 2022.
- [28] Gendi Liu, Ning Sun, Dingkun Liang, Yiheng Chen, Tong Yang, and Yongchun Fang. Neural network-based adaptive command filtering control for pneumatic artificial muscle robots with input uncertainties. *Control Engineering Practice*, 118:104960, 2022.
- [29] Niu Jianjun, Fu Yongling, and Qi Xiaoye. Design and application of discrete sliding mode control with rbf network-based switching law. *Chinese Journal of Aeronautics*, 22(3):279–284, 2009.
- [30] Hao Feng, Qianyu Song, Shoulei Ma, Wei Ma, Chenbo Yin, Donghui Cao, and Hongfu Yu. A new adaptive sliding mode controller based on the rbf neural network for an electro-hydraulic servo system. *ISA Transactions*, 129:472–484, 2022.
- [31] Wei He, Yuhao Chen, and Zhao Yin. Adaptive neural network control of an uncertain robot with full-state constraints. *IEEE Transactions on Cybernetics*, 46(3):620–629, 2016.
- [32] Wei He, Zichen Yan, Changyin Sun, and Yunan Chen. Adaptive neural network control of a flapping wing micro aerial vehicle with disturbance observer. *IEEE Transactions on Cybernetics*, 47(10):3452–3465, 2017.
- [33] Hongjun Yang and Jinkun Liu. An adaptive RBF neural network control method for a class of nonlinear systems. *IEEE/CAA Journal of Automatica Sinica*, 5(2):457–462, 2018.
- [34] Khalid Abidi, Jian-Xin Xu, and Yu Xinghuo. On the discrete-time integral sliding-mode control. *IEEE Transactions on Automatic Control*, 52(4):709–715, 2007.
- [35] Devika KB and Susy Thomas. Power rate exponential reaching law for enhanced performance of sliding mode control. *International Journal of Control, Automation and Systems*, 15:2636–2645, 2017.
- [36] Simon Fabri and Visakan Kadirkamanathan. *Functional Adaptive Control. An Intelligent Systems Approach*, volume 55. Springer London, 01 2001.
- [37] Shihua Li, Haibo Du, and Xinghuo Yu. Discrete-time terminal sliding mode control systems based on euler’s discretization. *IEEE Transactions on Automatic Control*, 59(2):546–552, 2014.
- [38] Céline Schreiber, and Florent Moissenet. A multimodal dataset of human gait at different walking speeds established on injury-free adult participants. *Scientific Data*, 66(1), 2019.